Phase transitions induced by confinement of ferroic nanoparticles

Anna N. Morozovska,[*,†] Maya D. Glinchuk,[‡] and Eugene A. Eliseev[*,§]
Institute for Problems of Materials Science, NAS of Ukraine, Krjijanovskogo 3, 03142 Kiev, Ukraine
(Received 26 March 2007; revised manuscript received 18 May 2007; published 2 July 2007)

A general approach for considering primary ferroic (ferroelectric, ferromagnetic, ferroelastic) nanoparticle phase transitions was proposed in phenomenological theory framework. The surface stress, order parameter gradient, and striction, as well as depolarization, demagnetization, and de-elastification effects, were included into the free energy. The strong intrinsic surface stress under the curved nanoparticle surface was shown to play the important role in the shift of transition temperature (if any) up to the appearance of a new ordered phase absent in the bulk ferroic. Euler-Lagrange equations obtained after the Landau-Ginzburg-Devonshire free energy minimization were solved by direct variational method. This leads to the conventional form of the free energy with renormalized coefficients depending on nanoparticle sizes, surface stress, and electrostriction tensor values, and so opens the way for polar property calculations by algebraic transformations. Surface piezoeffect causes built-in electric field that induces an electretlike polar state and smears the phase transition point. The approximate analytical expression for the size-induced ferroelectric transition temperature dependence on cylindrical or spherical nanoparticle sizes, polarization gradient coefficient, correlation radius, intrinsic surface stress, and electrostriction coefficient was derived. Under the favorable conditions (radius of 5–50 nm and compressive surface stress), spatial confinement induces a ferroelectric phase in incipient ferroelectric nanowires and nanospheres. The prediction of size-induced ferroelectricity in $KTaO_3$ nanorods with radius less than 5–20 nm at room temperature could be useful for the next generation of devices based on three-dimensional nanostructures.

DOI: 10.1103/PhysRevB.76.014102 PACS number(s): 77.80.−e, 77.84.Dy, 68.03.Cd, 68.35.Gy

I. INTRODUCTION

Until now, phase transitions in solids have attracted much scientific and technical interest because of the property anomalies in the vicinity of the phase transition temperature. Recently, the ability to govern the appearance of phase transitions at any arbitrary temperature has been demonstrated in nanosized materials due to the so-called size-driven phase transition. Such transitions were observed in many solids, including ferroelectric, ferromagnetic, and ferroelastic ones. Ferroelectric, ferromagnetic, and ferroelastic materials are known to belong to the primary ferroics,[1] because the application of an electric, a magnetic, or an elastic field higher than a coercive one leads to the switching of the corresponding order parameter. The common feature of nanomaterials with sizes less than 100 nm, such as films and nanoparticles of different shapes, is an essential influence of the surface on their properties. Allowing for all surface properties (including symmetry, electronic, photonic, etc.) different from those in the bulk nanomaterials opens the way for obtaining a variety of new unique properties,[2] a lot of which are useful for applications, e.g., the ability to store and release energy in well-regulated manners, making them very useful for sensors and actuators.

Among the different ferroic nanomaterials, the magnetic ones are the most thoroughly investigated, in particular, thin magnetic films and their multilayers.[1,3] The outlook of ferroelectric thin film applications in memory devices leads to the intensive investigations of their polar and dielectric property anomalies during the past decade.[4] Recently, the investigations of the cylindrical and spherical ferroic nanoparticles became a hot topic, because of the new behavior of their properties, absent in the bulk. For instance, room temperature ferromagnetism has been observed in spherical nanoparticles (size of 7–30 nm) of nonmagnetic oxides such as CeO_2, Al_2O_3, ZnO, etc.[2] Extremely strong superparamagnetic behavior down to 4 K has been found in gold and palladium nanoparticles, which are nonmagnetic in the bulk.[5] Particles of both metals had a narrow size distribution with a mean diameter of 2.5 nm. To the best of our knowledge the quantitative explanation and theoretical description of size-driven magnetism in nanoparticles are absent.

Keeping in mind the similarity of the ferroic properties, one could expect the appearance of ferroelectricity in highly polarizable paraelectric nanoparticles induced by spatial confinement. Unfortunately, nothing of this kind has been revealed up to now. The only encouraging result has been recently reported by Yadlovker and Berger.[6] They reported about the polarization enhancement and ferroelectric phase conservation in Rochelle salt (RS) nanorods of diameter of 30 nm up to material decomposition temperature of 55 °C, which is about 30 °C higher than the transition temperature of the bulk crystals. The phenomenological description of ferroelectricity enhancement in confined nanorods has been recently proposed.[7,8]

To check the possibility of the appearance of ferroelectricity in the nanoparticles of the materials, which are nonferroelectric in the bulk, as well as to reveal the common features responsible for the appearance of the new phases in primary ferroic nanoparticles, in this paper, we study phase transitions in them. The calculations have been performed in the phenomenological theory framework for the case of single-domain ferroics, which is known to be valid for small enough sizes (less than 100 nm).[1,9–13] We took into account the contribution of the surface stress into the free energy and the gradient of order parameter (magnetization, polarization, or strain), as well as depolarization, demagnetization, or de-elastification effects, since all these factors are known to influence strongly the phase transitions in nanomaterials. However, in most of the theoretical papers devoted to the

consideration of the size effects in spatially confined systems, the simultaneous influence of the aforementioned factors and especially surface stress on the phase transitions was neglected (see, e.g., Refs. 2 and 14–18).

Here, we have shown that phase transitions absent in the bulk appear in cylindrical or spherical ferroic nanoparticles under the favorable conditions. The detailed consideration was performed for incipient ferroelectric $KTaO_3$, which is paraelectric up to 0 K in the bulk. The theory predicts optimal sizes for appearance of ferroelectricity in incipient ferroelectric nanoparticles.

II. BASIC CONCEPTS FOR FERROIC NANOPARTICLES

When elaborating thermodynamic theory for the description of surface and size effects on polar properties and phase diagrams of ferroelectric nanoparticles of different shapes, we will use the Landau-Ginsburg-Devonshire phenomenological approach (see, e.g., Refs. 19–22) with respect to the surface energy, correlation (gradient) energy, depolarization field, and mechanical stress.

A characteristic feature of the phenomenological description of the nanoscale structures is the surface energy contribution that becomes comparable with the bulk one and can exceed it when size decreases.

For the case of primary ferroics, the Landau-Ginzburg-Devonshire expansion of the bulk (G_V) and surface (G_S) parts of the Gibbs free energy on the multicomponent order parameter $\boldsymbol{\eta}$ powers (vectors of polarization, magnetization, or strain tensor for ferroelectric, ferromagnetic, or ferroelastic media, respectively) and stress tensor components powers $\hat{\sigma}$ has the forms

$$G_V = \int_V d^3r \left[\frac{a_{ij}(T)}{2}\eta_i\eta_j + \frac{a_{ijkl}}{4}\eta_i\eta_j\eta_k\eta_l + \frac{a_{ijklmn}}{6}\eta_i\eta_j\eta_k\eta_l\eta_m\eta_n + \cdots + \frac{g_{ijkl}}{2}\left(\frac{\partial\eta_i}{\partial x_j}\frac{\partial\eta_k}{\partial x_l}\right) - \eta_i\left(E_{0i} + \frac{E_i^d}{2}\right) - Q_{ijkl}\sigma_{ij}\eta_k\eta_l - \frac{1}{2}s_{ijkl}\sigma_{ij}\sigma_{kl}\right], \quad (1a)$$

$$G_S = \int_S d^2r \left(\frac{a_{ij}^S}{2}\eta_i\eta_j + \frac{a_{ij}^S}{4}\eta_i^2\eta_j^2 + \frac{a_{ijk}^S}{6}\eta_i^2\eta_j^2\eta_k^2 - q_{ijkl}^S\sigma_{ij}\eta_k\eta_l + d_{ijk}^S\sigma_{jk}\eta_i + \mu_{\alpha\beta}^S s_{\alpha\beta jk}\sigma_{jk} + \frac{\nu_{ijkl}^S}{2}\sigma_{ij}\sigma_{kl} + \cdots \right). \quad (1b)$$

Coefficients $a_{ij}(T)$ explicitly depend on temperature T in the framework of the Landau-Ginzburg-Devonshire approach. Coefficients a_{ij}^S of the surface energy expansion may also depend on temperature.

High order expansion coefficients a_{ijkl}, a_{ijklmn}, a_{ijkl}^S, and a_{ijklmn}^S are supposed to be temperature independent; constants g_{ijkl} determine the magnitude of the gradient energy. Tensors g_{ijkl} and a_{ijklmn} are positively defined. The situation with tensor a_{ijkl} depends on the phase transition order, namely, tensor a_{ijkl} is positively defined for the second order phase transition, while for the first order ones, it is negatively defined. $\mathbf{E}_0$ is the external field conjugated with order parameter $\boldsymbol{\eta}$.

$\mathbf{E}^d$ is the depolarization, demagnetization, or de-elastification field that appears due to the nonzero divergence of order parameter $\boldsymbol{\eta}$ in a confined system [$\mathrm{div}(\boldsymbol{\eta}) \neq 0$]. It is easy to show that $\boldsymbol{\eta}$ and $\mathbf{E}_d$ are related to each other via the linear operator $\hat{N}^d[\boldsymbol{\eta}]$ as $\mathbf{E}^d \cong \hat{N}^d[\boldsymbol{\eta}]$.[19] In the general case of spatial inhomogeneity of the $\boldsymbol{\eta}$ operator, $\hat{N}^d[\boldsymbol{\eta}]$ has only an integral representation (see, e.g., Ref. 23). Field $\mathbf{E}^d$ tends to suppress the ordered phase inside the system.

Coupling terms $Q_{ijkl}\sigma_{ij}\eta_k\eta_l$ and $q_{ijkl}^S\sigma_{ij}\eta_k\eta_l$ determine the influence of mechanical stress on the order parameter for the materials with high symmetry paraphase (paraelectric, paramagnetic, or paraelastic). Here, Q_{ijkl} and q_{ijkl}^S are, respectively, the bulk and surface striction coefficients; s_{ijkl} are, components of the elastic compliance tensor.[24] The symmetry of surface striction tensor q_{ijkl}^S is the same as that of bulk striction Q_{jklm} one, but their signs and relative values can be different. For instance, anomalously large surface magnetostriction was observed in NiFe/Ag/Si, NiFe/Cu/Si, and Ni/SiO_2 thin films of thickness below about 5 nm.[25]

In Eq. (1b), surface piezoeffect tensor d_{ijk}^S is introduced. It arises even in cubic paraelectrics due to the symmetry breaking near the surface (vanishing of inversion center, see, e.g., Refs. 26 and 27), while in magnetics, it exists when there is no inversion of time among the symmetry operations of the material. Tensor ν_{jklm}^{Si} is related to the surface excess elastic moduli.

Intrinsic surface stress $\mu_{\alpha\beta}^S$ exists under the curved surface of a solid body and determines the excess pressure on the surface.[28,29] Surface stress tensor $\mu_{\alpha\beta}^S$ is defined as the derivative of the surface energy on the deformation tensor. Let us underline that in many experimental papers (e.g., Refs. 30–32), size effects of ferroelectric nanoparticles phase diagrams are related to the intrinsic surface stress (or surface tension by analogy with liquids). Intrinsic mechanical stress under a curved surface is determined by the tensor of intrinsic surface stress $\mu_{\alpha\beta}^S$:

$$n_k\sigma_{kj}|_S = -\frac{\mu_{\alpha\alpha}^S}{R_\alpha}n_j, \quad (2)$$

where R_α are the main curvatures of a surface free of facets and edges in continuum media approximation and n_k are components of the external normal.[28,29] In the case of mechanical stress homogeneous distribution, $\hat{\sigma} = -(\mu_{\alpha\alpha}^S/R_\alpha)\hat{L}$, where $\hat{L}$ is the second rank tensor with constant coefficients. The form of tensor $\hat{L}$ is determined by the nanoparticle shape (e.g., spherical, ellipsoidal, or cylindrical) and mechanical boundary conditions.

The sign of surface stress tensor components $\mu_{\alpha\beta}^S$ depends on the chemical properties of the nanoparticle ambient material and the presence of oxide or interface layer.[29] Taking into account that there exists surface layers or interfaces with chemical, structural, and polar properties different from those of the bulk, hereinafter, we consider both positive and negative values of $\mu_{\alpha\alpha}^S$.

For the considered case of nanoparticles with diameter less than 100 nm, stress $\hat{\sigma}$ can be considered as homogeneous. Its contributions into the renormalization of the qua-

dratic term coefficients in Eqs. (1) via striction effect is as follows:

$$a_{Rij}^S = \left[a_{ij}^S(T) + 2q_{lkij}^S L_{lk} \frac{\mu_{\alpha\alpha}^S}{R_\alpha} \right], \quad (3)$$

$$a_{Rij} = \left[a_{ij}(T) + 2Q_{lkij} L_{lk} \frac{\mu_{\alpha\alpha}^S}{R_\alpha} \right].$$

For the conventional ferroics, $a_{ij}(T)$ have the view $a_{ij}(T) = \delta_{ij}\alpha_T(T - T_C^i)$, where T_C^i is the Curie temperature of the bulk material for the order parameter component η_i. By neglecting $\mathbf{E}_d$ and gradient contribution, one obtains from Eq. (3) the Curie temperature renormalization:

$$T_{CR}^x = T_C^x - \frac{2\tau_x}{\alpha_T} \frac{\mu_{\alpha\alpha}^S}{R_\alpha}, \quad T_{CR}^y = T_C^y - \frac{2\tau_y}{\alpha_T} \frac{\mu_{\alpha\alpha}^S}{R_\alpha}, \quad (4)$$

$$T_{CR}^z = T_C^z - \frac{2\tau_z}{\alpha_T} \frac{\mu_{\alpha\alpha}^S}{R_\alpha},$$

where the constants $\tau_i = Q_{lkii} L_{lk}$ $(i = x, y, z)$ are introduced. It is seen that renormalized Curie temperatures T_{CR}^i are different. The shifts of T_{CR}^i that originated from surface stress $\hat{\sigma}$ lead not only to the change of the nanoparticle phase diagram in comparison with a bulk ferroic system but, under the favorable conditions (e.g., at $\tau_i \mu_{\alpha\alpha}^S < 0$ and $T_{CR}^i > 0$), to the appearance of the new phases absent in the bulk. In the particular case when a bulk cubic system transforms into the polar tetragonal phase with six possible orientations of order parameter (such as ferroelectric $PbTiO_3$ or multiferroic $BiFeO_3$) at $T < T_C$, the confined system subjected to the surface stress of arbitrary symmetry could transform into the polar phase with only two possible orientations of the order parameter (e.g., $\pm\eta_3$) corresponding to the component with the highest transition temperature (T_{CR}^z).

However, in order to obtain rigorous renormalization of the Curie temperature, one should take into consideration the renormalization of $a_{ij}(T)$ originating from the inner field $\mathbf{E}^d$ and order parameter gradient, so Eqs. (3) and (4) are valid only for the case when the surface stress contribution is much larger than the terms that originated from $\mathbf{E}^d \boldsymbol{\eta}$ and $g_{iiii}(\nabla \eta_i)^2$. It is not excluded, since the surface stress σ, existing in nanoparticles with radius of curvature $R = 5-50$ nm, is about 10^8-10^{10} Pa at the reasonable values of surface stress tensor $|\mu_{\alpha\alpha}^S| = 5-50$ N/m.[29,31] Therefore, the stress induced by surface curvature is very strong and so it may cause noticeable shift of the bulk phase transition temperature (if any).

Field $\mathbf{E}^d$ always leads to the decrease of the Curie temperature. However, it vanishes in some important cases, e.g., long nanorods with order parameter aligned along the cylinder axis[7,8] or magnetic particles with superconducting covering.

For the sake of rigorous consideration of all contributions into the Curie temperature, let us perform calculations for ferroic materials with definite characteristics. Namely, we will consider size-induced transitions between paraphase and ordered phases for the one component order parameter in cylindrical and spherical perovskite nanoparticles of conventional and incipient ferroelectrics.

To be sure that our efforts will not be in vain, let us perform simple estimations. It is obvious from Eq. (4) that the transition temperature shift depends on the $Q_{lkii}L_{lk}$ values and signs, and it increases with decrease of the particle radius. Typical bulk electrostriction coefficients Q_{lkij} are of order of magnitude of $0.1-0.05$ m^4/C^2, which leads to the estimation of surface stress via striction contribution into $a_{ij}(T)$ renormalization as $|2Q_{lkij}L_{lk}(\mu_{\alpha\alpha}^S/R)| \cong 10^7-10^9$ SI units; so $|T_{CR}^i - T_C^i| \sim 50-500$ K at $L_{lk} \sim 1$ and $\alpha_T \sim 10^6$ m/F K for $|\mu_{\alpha\alpha}^S| = 5-50$ N/m. Thus, under the favorable conditions, surface stress essentially increases the transition temperature and may induce ordered phase in incipient ferroelectrics.

III. FREE ENERGY FUNCTIONAL AND ELASTIC PROBLEM FOR NANOSIZED PEROVSKITES

For the perovskite symmetry, the Gibbs bulk free energy expansion [Eq. (1a)] on polarization P_3 and stress σ_{nm} powers has the form

$$G_V = \int_V d^3r \left[\frac{a_1(T)}{2} P_3^2 + \frac{a_{11}}{4} P_3^4 + \frac{a_{111}}{6} P_3^6 + \frac{g}{2} (\nabla P_3)^2 - P_3 \left(E_0 + \frac{E_3^d}{2} \right) - Q_{ij33}\sigma_{ij} P_3^2 - \frac{1}{2} s_{ijkl}\sigma_{ij}\sigma_{kl} \right]. \quad (5a)$$

Here, E_3^d and E_0 are the depolarization and external electric field z components.

The surface free energy [Eq. (1b)] polarization-dependent expansion has the form

$$G_S = \sum_i \int_{S_i} d^2r \left(\frac{a_1^{Si}}{2} P_3^2 + \frac{a_{11}^{Si}}{4} P_3^4 + \mu_{\alpha\beta}^{Si} s_{\alpha\beta jk}\sigma_{jk} + \frac{\nu_{jklm}^{Si}}{2} \sigma_{jk}\sigma_{lm} + d_{3jk}^{Si}\sigma_{jk} P_3 - q_{jk33}^{Si}\sigma_{jk} P_3^2 \right). \quad (5b)$$

Here, superscript Si numbered the surfaces; n_k is the normal to the surface; Greek characters label two-dimensional indices in the surface plane, whereas Roman indices are three-dimensional ones.

For the sake of simplicity, hereinafter, we consider the case of a mechanically isotropic solid, where the symmetry of surface stress tensors are isotropic, namely, $\mu_{\alpha\beta}^{Si} = \mu\delta_{\alpha\beta}$ for mechanically free nanoparticles (δ_{jk} is the Kronecker symbol).

The free energy [Eqs. (5)] is minimal when polarization P_3 and relevant stress tensor components σ_{jk} are defined at the nanostructure boundaries.[24] Under such conditions, one should solve the equation of state $\partial G / \partial \sigma_{jk} = -u_{jk}$, where u_{jk} is the strain tensor.

For the cases of the clamped system with defined displacement components (or with mixed boundary conditions), one should find the equilibrium state as the minimum of the Helmholtz free energy $F_V + F_S$ ($F_V = G_V + \int_V d^3r \cdot u_{jk}\sigma_{jk}$ and $F_S = G_S + \int_S d^2r \cdot u_\alpha \sigma_{\alpha k} n_k$) originating from the Legendre transformation of G.[33]

Equilibrium equations of state could be obtained after variation of the Helmholtz energy on displacement u_j, Gibbs

energy on stress σ_{ij}, polarization P_3, and its derivatives:

$$\frac{\partial \sigma_{ij}}{\partial x_i} = 0, \quad Q_{ij33}P_3^2 + s_{ijkl}\sigma_{kl} = u_{ij}, \tag{6a}$$

$$(a_1 - Q_{ij33}\sigma_{ij})P_3 + a_{11}P_3^3 + a_{111}P_3^5 - g\frac{\partial^2 P_3}{\partial x_{k^2}} = E_0 + E_3^d. \tag{6b}$$

Equations (6) should be supplemented by the boundary conditions for strain (or stress) and polarization. To the best of our knowledge the general solution of the coupled problem given by Eqs. (6) is absent. In what follows, we will use a decoupling approximation for mechanical and electrostatic equations allowing for the boundary conditions on the nanostructure surfaces.

A. Freestanding cylindrical particle

The boundary conditions [Eq. (2)] on the surface of a cylindrical rod of radius R in the cylindrical coordinates (r, φ, z) have the following forms:

$$\sigma_{\rho\rho}|_{\rho=R} = -\frac{\mu}{R}, \quad \sigma_{\rho\varphi}|_{\rho=R} = 0, \quad \sigma_{\rho z}|_{\rho=R} = 0,$$

$$\sigma_{zz}|_{z=\pm h/2} = 0, \quad \sigma_{z\rho}|_{z=\pm h/2} = 0, \quad \sigma_{z\varphi}|_{z=\pm h/2} = 0. \tag{7}$$

The equation $\partial\sigma_{ij}/\partial x_i = 0$ in the bulk of the cylindrical body along with the boundary conditions [Eq. (7)] can be fulfilled with a uniform solution. The stress and strain tensor components have the following forms:

$$\sigma_{\rho\rho} = \sigma_{\varphi\varphi} = \sigma_{11} = \sigma_{22} = -\frac{\mu}{R},$$

$$\sigma_{\rho\varphi} = \sigma_{\rho z} = \sigma_{zz} = \sigma_{z\varphi} = \sigma_{12} = \sigma_{13} = \sigma_{23} = \sigma_{33} = 0. \tag{8}$$

B. Freestanding spherical particle

The boundary conditions [Eq. (2)] on the surface of a spherical particle of radius R have the following forms in the spherical coordinates (r, θ, φ):

$$\sigma_{rr}|_{r=R} = -\frac{2\mu}{R}, \quad \sigma_{r\varphi}|_{r=R} = 0, \quad \sigma_{r\theta}|_{r=R} = 0. \tag{9}$$

The equation $\partial\sigma_{ij}/\partial x_i = 0$ in the bulk of the spherical body along with the boundary conditions [Eq. (9)] can be fulfilled with a uniform solution. The stress and strain tensor components have the following forms:

$$\sigma_{rr} = \sigma_{\theta\theta} = \sigma_{\varphi\varphi} = \sigma_{11} = \sigma_{22} = \sigma_{33} = -\frac{2\mu}{R},$$

$$\sigma_{r\theta} = \sigma_{r\varphi} = \sigma_{12} = \sigma_{13} = \sigma_{23} = 0. \tag{10}$$

IV. EULER-LAGRANGE EQUATION FOR A CYLINDRICAL NANOPARTICLE IN AMBIENT CONDITIONS

Let us consider a ferroelectric cylindrical nanoparticle with radius R, height h, and axisymmetric polarization $P_3(\rho, z)$ oriented along the z axes. The external electric field is $\mathbf{E} = (0, 0, E_0)$ (see Fig. 1).

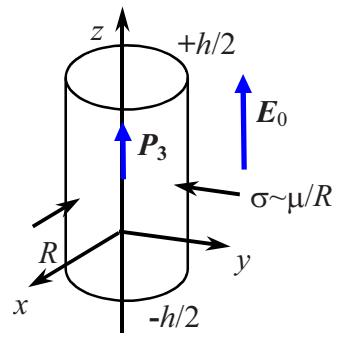

FIG. 1. (Color online) Geometry of a cylindrical particle.

For a perovskite ferroelectric nanorod with polarization $P_3(\rho)$, the substitution of solution (8) into the free energy [Eqs. (5)] gives the expression for the polarization-dependent part:

$$G_V = h\int_0^R rdr\left[\left(\frac{a_1}{2} + 2Q_{12}\frac{\mu}{R}\right)P_3^2 + \frac{a_{11}}{4}P_3^4 + \frac{a_{111}}{6}P_3^6 + \frac{g}{2}\left(\frac{\partial}{\partial\rho}P_3\right)^2 - P_3\left(E_0 + \frac{E_d}{2}\right)\right], \tag{11a}$$

$$G_S = hR\left[\left(\frac{a_1^S}{2} + 2q_{12}^S\frac{\mu}{R}\right)P_3^2(R) + \frac{a_{11}^S}{4}P_3^4(R) - 2d_{31}^S\frac{\mu}{R}P_3(R)\right]. \tag{11b}$$

Hereinafter, we neglect depolarization field E_d for the case $h \gg R$ of the considered long nanorods (nanowires). Variation of the free energy [Eqs. (11)] leads to the Euler-Lagrange equation for the polarization $P_3(\rho)$:

$$\left(a_1 + 4Q_{12}\frac{\mu}{R}\right)P_3(\rho) + a_{11}P_3^3(\rho) + a_{111}P_3^5(\rho) - g\frac{1}{\rho}\frac{\partial}{\partial\rho}\rho\frac{\partial}{\partial\rho}P_3(\rho) = E_0,$$

$$\left[P_3 + \lambda_S\left(\frac{dP_3}{d\rho} + \frac{a_{11}^S}{g}P_3^3\right)\right]\Bigg|_{\rho=R} = -P_d, \tag{12}$$

where the boundary conditions have been rewritten via renormalized characteristic length λ_S and surface polarization P_d, namely:

$$\lambda_S^{-1}(R) = \frac{a_1^S}{g} + \frac{4q_{12}^S}{g}\frac{\mu}{R}, \tag{13a}$$

$$P_d(R) = -\frac{2\mu}{R}d_{31}^S\frac{\lambda_S}{g}. \tag{13b}$$

It is worthwhile to underline that characteristic length λ_S could be negative or positive, since the signs of a_1^S and q_{12}^S are not predetermined. When the surface piezoelectric effect could be absent (i.e., $P_d = 0$), then characteristic length λ_S had the meaning of extrapolation length. Introducing the param-

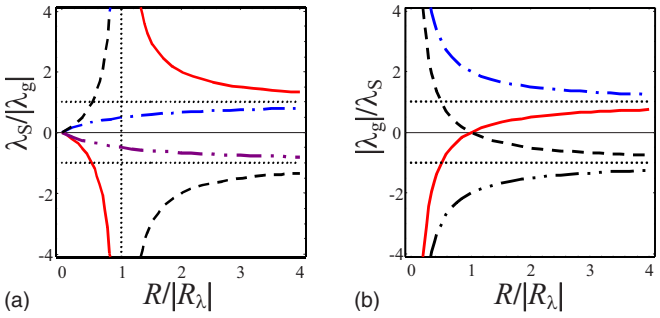

FIG. 2. (Color online) (a) Characteristic length $\lambda_S/|\lambda_g|$ and (b) $|\lambda_g|/\lambda_S$ vs nanowire radius $R/|R_\lambda|$ for $\lambda_g>0$ and $R_\lambda>0$ (solid curves), $\lambda_g<0$ and $R_\lambda>0$ (dashed curves), $\lambda_g>0$ and $R_\lambda<0$ (dash-dotted curves), and $\lambda_g<0$ and $R_\lambda<0$ (double-dash-dotted curves).

eters $R_\lambda=-4q_{12}^S\mu/a_1^S$ and $\lambda_g=g/a_1^S$, one obtains that $\lambda_S^{-1}(R)=\lambda_g^{-1}(1-R_\lambda/R)$. The size dependence of the normalized characteristic length $\lambda_S/|\lambda_g|$ is shown in Fig. 2. It is clear that $\lambda_S/|\lambda_g|$ is negative at $\mu>0$ and $R<R_\lambda$, as should be expected from Eq. (13a).

It should be noted that some authors (see, e.g., Refs. 15–17) also considered the size-dependent characteristic (extrapolation) length that was derived from microscopic models and thus could be related to surface stress considered here in the phenomenological framework.

Application of the direct variational method for the approximate solution of the Euler-Lagrange equation [Eq. (12)], as was described earlier,[7,34] leads to the conventional form of the free energy with renormalized coefficients. In particular, surface polarization P_d in the boundary conditions [Eq. (12)] leads to the appearance of the built-in field E_{cyl} that induces an electretlike polar state at $R<R_{cr}$ (instead of a conventional paraelectric phase) and smears the dielectric permittivity maximum in the phase transition point. The electretlike state possesses piezoelectric and pyroelectric properties, but hysteresis loops are absent.[35] For a cylindrical nanoparticle, the built-in field has the form

$$E_{cyl}(R)\approx -\frac{4\mu}{R^2}d_{31}^S. \tag{14}$$

One can see from Eq. (14) that the built-in field is proportional to the surface stress tensor μ and piezoelectric coefficients d_{31}^S; it increases with decrease of radius.

The transcendental equation for the determination of the Curie temperature $T_{cyl}(R)$ at a given radius R, as well as for the critical radius $R_{cyl}(T)$ at a given temperature T, which corresponds to the second order phase transition from the ferroelectric to the paraelectric phase (at $E_{cyl}=0$) or electretlike state (at $E_{cyl}\neq 0$) acquires the form

$$J_0\left[R\sqrt{-\frac{a_R(T,R)}{g}}\right] - \lambda_S(R)\sqrt{-\frac{a_R(T,R)}{g}}J_1\left[R\sqrt{-\frac{a_R(T,R)}{g}}\right]=0, \tag{15}$$

where J_0 and J_1 are Bessel functions of the zero and first orders correspondingly, $a_R(T,R)=a_1(T)+4Q_{12}\frac{\mu}{R}$.

A. Ferroelectricity enhancement in conventional ferroelectric nanorods

For *conventional* ferroelectrics, Padé approximations of the solution of Eq. (15) for $T_{cyl}(R)$ could be rewritten as

$$T_{cyl}(R)\approx\begin{cases} T_C-\dfrac{4Q_{12}}{\alpha_T}\dfrac{\mu}{R}-\dfrac{g}{\alpha_T}\dfrac{2}{R\lambda_S(R)+2R^2/k_{01}^2}, & \lambda_S(R)\geq 0 \\ T_C-\dfrac{4Q_{12}}{\alpha_T}\dfrac{\mu}{R}-\dfrac{g}{\alpha_T}\left[\dfrac{2}{R\lambda_S(R)}-\dfrac{1}{\lambda_S^2(R)}\right], & \lambda_S(R)<0, \end{cases} \tag{16}$$

where $k_{01}=2.408\cdots$ is the smallest positive root of the equation $J_0(k)=0$. Note that at $\lambda_S\to 0$, Eq. (16) reduces to the one obtained in Refs. 7 and 8.

Under the condition $q_{12}^S=0$, we derived the following approximate expression for the critical radius $R_{cyl}(T)$ at a given temperature T

$$R_{cyl}(T)\approx\begin{cases} -\dfrac{k_{01}^2}{4}\lambda_g-\dfrac{2Q_{12}\mu}{a_1(T)}\pm\sqrt{\left[\dfrac{k_{01}^2}{4}\lambda_g-\dfrac{2Q_{12}\mu}{a_1(T)}\right]^2-\dfrac{g}{a_1(T)}\dfrac{k_{01}^2}{4}}, & \lambda_g\geq 0 \\ \dfrac{2(g\lambda_g+2Q_{12}\mu\lambda_g^2)}{g-a_1(T)\lambda_g^2}, & \lambda_g<0. \end{cases} \tag{17}$$

It is obvious that physically relevant values of the critical radius should be positive. That is why $\pm$ signs before the radical correspond to the different conditions. Namely, at $Q_{12}\mu<0$ and $a_1(T)<0$ or $Q_{12}\mu>0$ and $a_1(T)>0$ only the "+" sign makes sense, while at $Q_{12}\mu<0$ and $a_1(T)>0$, both "$\pm$" signs have sense and both critical radii define the region where ferroelectricity exists. In the case $(g+2Q_{12}\mu\lambda_S)<0$ and $\lambda_S\geq 0$, the region of $T_{cyl}(R)>T_C$ may extend down to

$R=0$. The simplest expression corresponds to the case $\lambda_S=0$ [i.e., $q_{12}^S=0$ and $a_1(T)=0$], when $R_{cyl}(T) \approx -\frac{2Q_{12}\mu}{a_1(T)} \pm \sqrt{\left[\frac{2Q_{12}\mu}{a_1(T)}\right]^2 - \frac{g}{a_1(T)}\frac{k_{01}^2}{4}}$.

Hereinafter, we consider the most favorable case $\mu Q_{12} < 0$ for ferroelectricity conservation in perovskite nanowires. It is seen from Eqs. (16) and (17) that the tension radii $R_\mu = -4Q_{12}\mu/\alpha_T T_C$ and $R_\lambda = -4q_{12}^S\mu/a_1^S$, length $\lambda_g = g/a_1^S$, and bulk correlation radius at zero temperature $R_S = \sqrt{g/\alpha_T T_C}$ (Ref. 20) determine the phase diagram. Note that no restrictions are known for phenomenological parameters R_λ and λ_g, since the quantity a_1^S can take arbitrary values. Ferroelectric phase transition temperature T_{cyl}/T_C vs radius R/R_S for different R_μ/R_S ratios and parameters R_λ/R_S and λ_g/R_S determining $\lambda_S^{-1}(R)=\lambda_g^{-1}(1-R_\lambda/R)$ dependence is depicted in Fig. 3.

The most interesting result is the transition temperature enhancement $T_{cyl} \gg T_C$ at small radius $R \ll R_S$ (see curves 4 and 5 in Fig. 3). The case corresponds to the so-called surface polar state,[23] appearing at negative λ_S values. However, under the condition $a_1^S > 0$, λ_S is positive at $R > R_\lambda$, and $\lambda_S \to g/a_1^S$ at $R \to \infty$, in accordance with Eq. (13a); the electrostriction term $\sim Q_{12}\mu/R$ vanishes at $R \to \infty$, making it clear that no ferroelectricity enhancement appears in the bulk.

As one could expect, there is a wide range of R/R_S values where $T_{cyl}/T_C < 1$ for the chosen parameters including the point $T_{cyl}=0$ (see Fig. 3). The point corresponds to the minimal critical radius $R_{cyl}(0)$ of the size-driven ferroelectric phase transition.

Under the favorable conditions, size effects (confined geometry) enhance ferroelectricity in conventional ferroelectrics. In particular, for nanowires of radius $R/R_S < 2-5$ at relatively large R_λ/R_S and R_μ/R_S values, the ratio $T_{cyl}/T_C > 1$ and it increases with decrease of R/R_S. Note that the values of R_μ and R_λ are defined by the surface stress coefficient μ, bulk Q_{12}, and surface q_{12}^S electrostriction coefficients, respectively. Therefore, exactly these quantities are responsible for the ferroelectricity enhancement in nanowires. The increase of T_{cyl} with increase of $\lambda_g/R_S \sim \sqrt{g}$ may reflect the importance of the polarization gradient contribution.

It is clear that size effects are most pronounced in the region $R < 10R_S$ that typically corresponds to the nanowire radius less than 50 nm since $R_S \sim 5-50$ Å; at that, the region width and the ratio T_{cyl}/T_C increase with the values of R_μ and/or R_λ; the latter parameters reflect the contribution of the surface stress.

As it has been already mentioned in the Introduction, the most striking observation of ferroelectricity enhancement and conservation in long nanorods (radius of 15 nm, length of 500 nm) has been reported by Yadlovker and Berger.[6] Besides ferroelectricity conservation up to Rochelle salt decomposition temperature that was explained earlier,[7,8] the authors measured the temperature dependence of remnant polarization $P_{SV}(T)$, hysteresis loops, and switching time τ_S. These polar properties can be calculated by a conventional way on the basis of the free energy with renormalized coefficients:

$$G \approx \left\{ \alpha_T[T - T_{cyl}(R)]\frac{P_{3V}^2}{2} + a_{11}\frac{P_{3V}^4}{4} + a_{111}\frac{P_{3V}^6}{6} - P_{3V}[E_0 + E_{cyl}(R)] \right\}. \quad (18)$$

Under the condition of negligibly small surface piezoeffect, it is easy to obtain from [Eq. (18)] that the spontaneous polarization is $P_{SV} \approx \sqrt{\alpha_T[T_{cyl}(R)-T]/a_{11}}$ and thermodynamic coercive field is $E_C^T = (2P_{SV}/3\sqrt{3})\alpha_T[T-T_{cyl}(R)]$. The thermodynamic coercive field corresponds to the case of nanorod homogeneous (monodomain) switching. In the case of inhomogeneous switching process, the activation field E_{cr}^a necessary for domain nucleus onset determines the observed coercive field E_C and switching time.[20] For the latter case, renormalized coefficient $\alpha_T[T-T_{cyl}(R)]$ should be included into the domain wall energy, spontaneous polarization, dielectric permittivity, etc., instead of the bulk coefficient $a_1(T)$, in order to describe adequately the domain nucleation stage and further domain wall motion (see Appendix A in Ref. 36 and Refs. 37 and 38 for details about nucleation and domain wall motion stages).

The applicability of our model to the description of phase transition between cubic paraelectric and tetragonal ferroelectric phases in ferroelastic-ferroelectric RS is valid only in the temperature range where RS ferroelectric properties can be described by the phenomenological framework. Moreover, we neglected the piezoelectric effect with respect to the shear stress in the paraelectric phase of RS since the effective surface tension creates no tangential stresses.

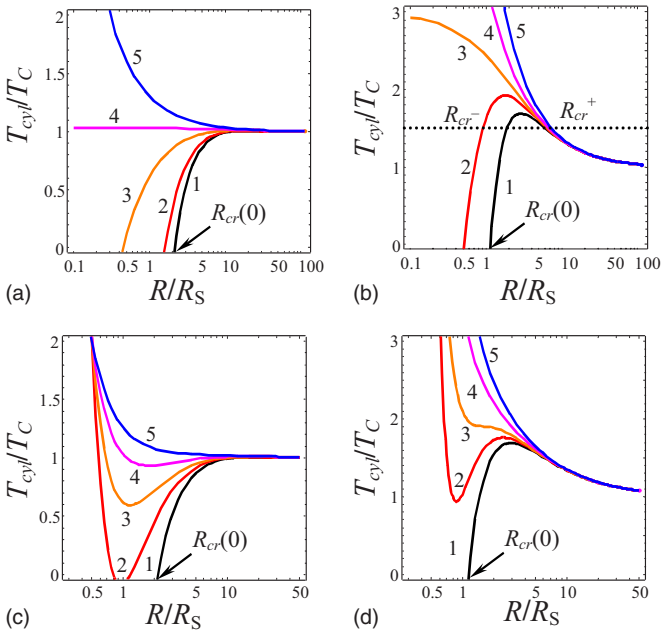

FIG. 3. (Color online) Ferroelectric phase transition temperature T_{cyl}/T_C vs R/R_S for (a) $R_\lambda/R_S=0$, $R_\mu/R_S=0.5$, and $\lambda_g/R_S=0,0.5,2,4,10$ (curves 1, 2, 3, 4, 5); (b) $R_\lambda/R_S=0$, $R_\mu/R_S=4$, and $\lambda_g/R_S=0,0.3,0.5,1,4$ (curves 1, 2, 3, 4, 5); (c) $R_\lambda/R_S=0.5$, $R_\mu/R_S=0.5$, and $\lambda_g/R_S=0,0.5,1,2,4$ (curves 1, 2, 3, 4, 5); (d) $R_\lambda/R_S=0.5$, $R_\mu/R_S=4$, and $\lambda_g/R_S=0,0.1,0.2,0.5,1$ (curves 1, 2, 3, 4, 5).

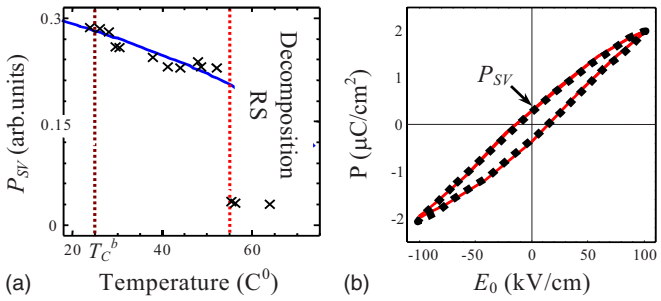

FIG. 4. (Color online) The dependence of remnant polarization $P_{SV}(T)$ on (a) temperature and (b) hysteresis loop of RS nanorods with radius $R=15$ nm. Symbols are experimental data from Ref. 6: (a) remnant polarization at applied field amplitude $E_0^{\max}=30$ kV/cm; (b) hysteresis loop at applied field frequency of 1 kHz and $T=21$ °C. Solid curves are theoretical calculations with parameters (a) $T_{cyl}=80$ °C, and $|E_{cyl}|\approx 2$ kV/cm and (b) $P_{SV}\approx 0.28$ μC/cm^2 and $E_C\approx 13$ kV/cm.

Despite the aforementioned limitations, let us perform quantitative comparison with experimental data for RS. The comparison of experimentally obtained polarization temperature dependence $P_{SV}(T)$ and hysteresis loop $P_{SV}(E_0)$ (symbols) in Ref. 6 with theoretical calculations (solid curves) are presented in Fig. 4.

The dependence $P_{SV}(T)$ was calculated from the equation $\alpha_T[T-T_{cyl}(R)]P_{3V}+a_{11}P_{3V}^3\approx E_{cyl}(R)$ for RS material parameters [see Fig. 4(a)].

The activation field value $E_{cr}^a\approx 13$ kV/cm calculated in Appendix A of Ref. 36 is very close to the experimentally obtained coercive field $E_C\approx 13.6$ kV/cm.[6] This means that thermal fluctuations $\sim k_BT$ cause rapid nanodomain nucleation in the nanorod under applied field $E_{cr}^a\approx 13$ kV/cm, in contrast to the switching of the bulk sample with much smaller coercive fields about 0.2 kV/cm.[20] Using the value $P_{SV}\approx 0.28$ μC/cm^2 calculated at $T=21$ °C as a remnant polarization [see Fig. 4(a)] and the value $E_{cr}^a\approx 13$ kV/cm as a coercive field, we modeled hysteresis loop $P_{SV}(E_0)$ from a conventional kinetic equation[20] [see Fig. 4(b)].

Using RS material parameters $g\approx 9\times 10^{-11}$ m^3/F,[39] $\alpha_T\approx 7.74\times 10^7$ m/F K, $T_C=297$ K, $a_{11}=3.36\times 10^{15}$ SI units (estimated from bulk polarization of RS crystal at room temperature, $P_S=\sqrt{\alpha_T T_r/a_{11}}\approx 0.25$ μC/cm^2), the sum $Q_{12}+Q_{13}=-0.63$ m^4/C^2 (instead of $2Q_{12}$ for perovskites), radius $R=15$ nm, and the value $T_{cyl}=80$ °C in Eq. (16), we obtained the estimation for surface stress coefficient $\mu\approx 25$ N/m. Note that it is the upper estimation (i.e., $\mu\leqslant 25$ N/m) since the third term in Eq. (16) appeared either positive at negative values λ_S or negligibly small at $\lambda_S\geqslant 0$, allowing for the small polarization gradient coefficient value g. Unfortunately, we could not find any experimental data concerning surface piezoeffect d_{ij}^S in RS, so we regard built-in field $E_{cyl}\sim d_{31}^S$ as a fitting parameter and obtained that $|E_{cyl}|\leqslant 2$ kV/cm and thus $d_{31}^S\approx 7.2\times 10^{-16}$ m^2/V. It is seen that theory fitted experimental data rather well at reasonable values of surface stress.

Yadlovker and Berger[6] observed the domains aligned along the nanorod axis. Thus, the important question is: how the expected theoretical results may change due to the presence of multiple nanodomains in the nanoparticles. In Ref. 7 we have shown that the domain splitting decreases the depolarization field inside the nanorod of finite length. Nanodomain formation would be energetically preferable until the depolarization energy decrease caused by the appearance of domains would be greater than the increase of domain wall correlation energy. Typically, depolarization field decreases the phase transition temperature; thus, nanodomain formation may increase it.

The domain nucleation and growth govern the nanorod switching in external electric field. In Appendix A of Ref. 36 we considered RS nanorod switching at applied homogeneous electric field (i.e., between two plain electrodes) within the framework of the Landauer model[40] for nanodomain nucleation. The preliminary results obtained here (we neglected pinning effects at nucleation stage) predicted that domain nucleation is rapid in comparison with the following domain wall growth. Since RS nanorods were prolate ($h\gg R$), the domain wall growth is mainly vertical, and so the wall one-dimensional velocity $\vartheta\sim\sqrt{E_0 h}$, described by the kinetic energy conservation law, is in agreement with the power law for the switching time $\tau_S\cong h/\vartheta\sim\sqrt{1/E_0}$ obtained from experimental data fitting in Ref. 6.

It is worthwhile to mention that some other experimental results indirectly speak in favor of the ferroelectricity enhancement and conservation in $PbZr_{0.52}Ti_{0.48}O_3$ nanorods with diameter less than 10–20 nm (Refs. 41 and 42) in single-crystalline $PbZr_{0.2}Ti_{0.8}O_3$ nanowires of elliptic cross section with main diameters of 70 and 180 nm.[32]

The developed phenomenological approach describes the observed peculiarities of ferroelectric nanorods.

B. Size-induced ferroelectricity in incipient ferroelectric nanowires

The Barrett formula $a_1(T)=\alpha_T[T_q/2\coth(T_q/2T)-T_0]$ is valid for *both* incipient and conventional ferroelectrics[43] at a wide temperature interval including low (quantum) temperatures. At temperatures $T\gg T_q/2$, the Barrett formula transforms into the classical form $a_1(T\gg T_q)\approx\alpha_T(T-T_0)$.

The transition temperature (induced by surface and size effects) is given by

$$T_{cyl}(R)\approx\begin{cases}\dfrac{T_q}{2}\left(\operatorname{arccoth}\left\{\dfrac{2}{T_q}\left[T_0-\dfrac{4Q_{12}}{\alpha_T}\dfrac{\mu}{R}-\dfrac{g}{\alpha_T}\dfrac{2}{R\lambda_S(R)+2R^2/k_{01}^2}\right]\right\}\right)^{-1}, & \lambda_S(R)\geqslant 0\\ \dfrac{T_q}{2}\left[\operatorname{arccoth}\left(\dfrac{2}{T_q}\left\{T_0-\dfrac{4Q_{12}}{\alpha_T}\dfrac{\mu}{R}-\dfrac{g}{\alpha_T}\left[\dfrac{2}{R\lambda_S(R)}-\dfrac{1}{\lambda_S^2(R)}\right]\right\}\right)\right]^{-1}, & \lambda_S(R)<0.\end{cases}\tag{19}$$

Using the asymptotic relation $[\text{arccoth}(x)]^{-1} \to x$ for $x \gg 1$, one can obtain that at temperatures $T \gg T_q/2$, Eq. (19) tends to Eq. (16) after the substitution $T_C \to T_0$, where $T_0 \leqslant 0$ is possible.

It is worth to underline that the second term in square brackets in Eq. (19) represents the contribution of biaxial stress originating from the intrinsic surface stress.

Note that approximate expressions [Eq. (17)] for the critical radius $R_{cyl}(T)$ are valid after substitution of the Barrett formula for $a_1(T)$.

Let us introduce tension radius $R_\mu = -4Q_{12}\mu/\alpha_T|T_0|$, bulk correlation radius $R_S = \sqrt{g/\alpha_T|T_0|}$, and ratio $T_q/2T_0$. The dependence of the temperatures $T_{cyl}/|T_0|$ vs radius R/R_S is depicted in Fig. 5.

It is clear that under the favorable conditions, size effects induce ferroelectric phase in incipient ferroelectrics. In particular, in nanorods with small enough ratio $R/R_S < 0.5$ and relatively large R_μ/R_S ratio, the ratio $T_{cyl}/|T_0| \gg 1$; also, the transition temperature essentially increases with decrease of R/R_S. The cross point of the curves in plot (b) corresponds to the point $R = R_\lambda$, where all lengths λ_S diverge in accordance with Eq. (13a) and so the transition temperature becomes equal.

Usually, T_0 is small enough and about 10–50 K. However, under the condition $T_{cyl}/|T_0| > 10$ (see horizontal lines in Fig. 5), size-induced ferroelectricity may exist at room temperatures. Allowing for small values of T_0 for incipient ferroelectric and large values of correlation radius R_S (from several to tens of lattice constant), the typical range $0 < R/R_S < 1$ (where $T_{cyl}/|T_0| > 0$) may be rather wide: from dozens to hundreds of lattice constants.

It is worth to underline that under the condition $Q_{12} < 0$, bi- and uniaxial stresses stimulate ordered phase appearance in incipient ferroelectrics. Really, Uwe and Sakudo[44] have found that the uniaxial stress higher than 5.25×10^8 Pa induces ferroelectric phase transition in bulk $KTaO_3$ at the temperature of 2 K. The same radial stress $\sigma = \mu/R$ appeared in $KTaO_3$ nanowires of radius $R = 4-40$ nm at the surface stress values $\mu = 4-40$ N/m,[29,31] reasonable for perovskites. This means that surface stress existing under the curved surface of $KTaO_3$ nanorod could induce ferroelectricity.

Let us consider the appearance of the size-induced ferroelectric phase in $KTaO_3$ nanowires quantitatively. We used

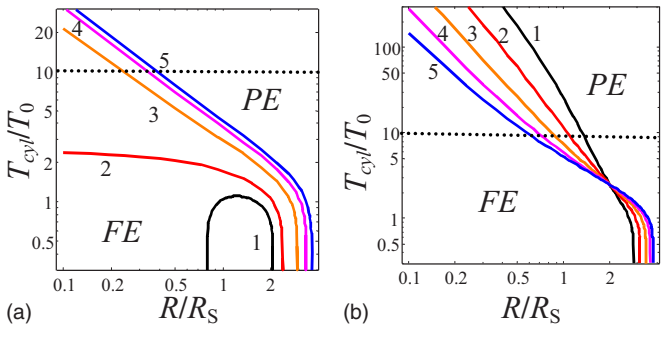

FIG. 5. (Color online) Ferroelectric phase transition temperature $T_{cyl}/|T_0|$ vs R/R_S for incipient ferroelectric at $\lambda_S^{-1}(R) = \lambda_g^{-1}(1 - R_\lambda/R)$, $T_q/2T_0 = 2$, and (a) $R_\mu/R_S = 4$, $R_\lambda/R_S = 0$, and $\lambda_g/R_S = 0.4, 0.5, 1, 2, 4$ (curves 1, 2, 3, 4, 5) and (b) $R_\lambda/R_S = 2$ and $\lambda_g/R_S = 0.25, 0.5, 1, 2, 4$ (curves 1, 2, 3, 4, 5).

Eq. (19) for the transition temperature; electrostriction constant Q_{12} was evaluated from the experiments.[44] Ferroelectric phase transition temperature T_{cyl} vs nanowire radius R for $KTaO_3$ is shown in Fig. 6.

Part (a) corresponds to the case when characteristic length $\lambda_S \to +\infty$ (i.e., $q_{12}^S = 0$ and $\lambda_g \to +\infty$) and so polarization gradient can be neglected, and radius dependence of T_{cyl} is caused by the surface stress only. Parts (b) and (c) correspond to the case when both surface stress and polarization gradient contribute into the transition temperature, but surface electrostriction is absent, i.e., $q_{12}^S = 0$ and so $\lambda_S = \lambda_g = \text{const}$. It is clear that negative λ_S increases the transition temperature in comparison with the positive ones [compare parts (b) and (c)]. Part (d) shows the influence of negative surface electrostriction on T_{cyl}. The cross point of the curves in plot (d) corresponds to the point $R = R_\lambda$, where all characteristic lengths diverge in accordance with Eq. (13a).

The prediction of size-induced ferroelectricity in $KTaO_3$ nanorods of radius less than 5–20 nm (see vertical lines in Fig. 6) at room temperatures (see horizontal lines in Fig. 6) could be very important for applications. Since $Q_{12} < 0$, the effect is possible for positive intrinsic surface stress coefficient μ that compresses the particle. An additional desirable condition is the negative length λ_S, possible even at $\lambda_g > 0$ for nanoparticle radius $R < R_\lambda$ when $\mu q_{12}^S < 0$.

Thus, we came to the conclusion about size-induced ferroelectricity in incipient ferroelectric $KTaO_3$ at room temperature for small enough nanowires. It is obvious that the same size-induced transition could be found in another incipient ferroelectric, $SrTiO_3$.

V. EULER-LAGRANGE EQUATION FOR A SPHERICAL NANOPARTICLE IN AMBIENT CONDITIONS

Let us consider a ferroelectric perovskite spherical nanoparticle of radius R and polarization $P_3(r)$ oriented along the z axes. The external electric field is $\mathbf{E} = (0, 0, E_0)$ (see Fig. 7).

For a sphere with polarization $P_3(r)$, substitution of solution (8) into the free energy [Eqs. (5)] leads to the following expression for the polarization-dependent part:

$$G_V = \int_0^R r^2 dr \left\{ \left[\frac{a_1}{2} + (Q_{11} + 2Q_{12}) \frac{2\mu}{R} \right] P_3^2 + \frac{a_{11}}{4} P_3^4 + \frac{a_{111}}{6} P_3^6 + \frac{g}{2} \left(\frac{\partial}{\partial r} P_3 \right)^2 - P_3 \left(E_0 + \frac{E_3^d}{2} \right) \right\}, \tag{20a}$$

$$G_S = R^2 \left\{ \left[\frac{a_1^S}{2} + (2q_{12}^S + q_{11}^S) \frac{2\mu}{R} \right] P_3^2(R) + \frac{a_1^S}{2} P_3^4(R) - (2d_{31}^S + d_{33}^S) \frac{2\mu}{R} P_3(R) \right\}. \tag{20b}$$

Here, the depolarization field is $E_3^d = n_d (\bar{P}_3 - P_3)$, where $\bar{P}_3$ stands for the spatial average on the sample volume, $n_d = 4\pi/1 + 2\varepsilon_e$ is a depolarization factor, and ε_e is the nanoparticle ambient dielectric permittivity.[45] Variation of the free energy [Eqs. (20)] leads to the Euler-Lagrange equation for polarization $P_3(r)$:

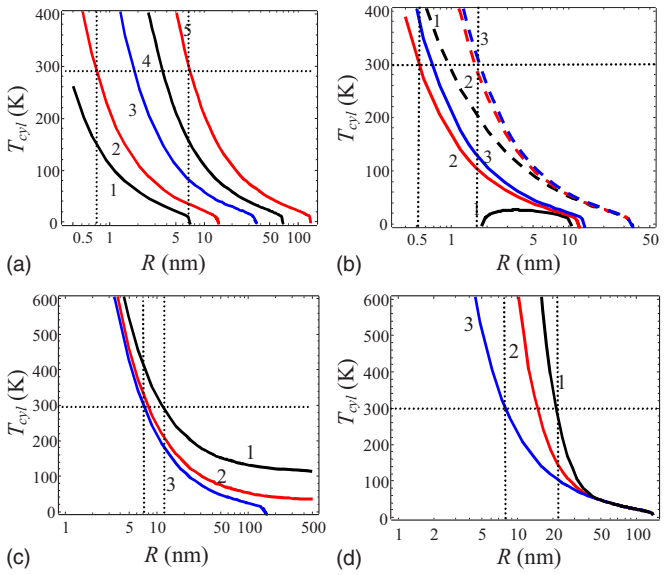

FIG. 6. (Color online) Ferroelectric phase transition temperature T_{cyl} vs nanowire radius R for $KTaO_3$ material parameters $T_q=55$ K, $T_0=13$ K, Curie-Weiss constant $C_{CW}=5.6\times10^4$ K, and $Q_{12}=-0.023$ m^4/C^2; gradient coefficient $g=10^{-10}$ V m^3/C in SI and $\lambda_S^{-1}(R)=\lambda_g^{-1}(1-R_\lambda/R)$. (a) $\lambda_g\to+\infty$, $R_\lambda=0$, and different surface stress values μ: 2, 4, 10, 20, 40 N/m (curves 1, 2, 3, 4, 5); (b) $\mu=4$ N/m (solid curves) and $\mu=10$ N/m (dashed curves), $R_\lambda=0$, and $\lambda_g=0.6,4,40$ nm (curves 1, 2, 3); (c) $\mu=40$ N/m, $R_\lambda=0$, and $\lambda_g=-1,-2,-10$ nm (curves 1, 2, 3); (d) $\mu=40$ N/m, $R_\lambda=50$ nm, and $\lambda_g=1,2,10$ nm (curves 1, 2, 3).

$$\left[a_1+(Q_{11}+2Q_{12})\frac{4\mu}{R}\right]P_3(r)+a_{11}P_3^3(r)+a_{111}P_3^5(r)$$
$$-\frac{g}{r^2}\frac{\partial}{\partial r}r^2\frac{\partial}{\partial r}P_3(r)=E_0+E_3^d,$$
$$\left[P_3+\lambda_S\left(\frac{dP_3}{dr}+\frac{a_{11}^S}{g}P_3^3\right)\right]\Bigg|_{r=R}=-P_d. \quad (21)$$

Here, the boundary conditions have been rewritten via renormalized length λ_S and surface polarization P_d, namely:

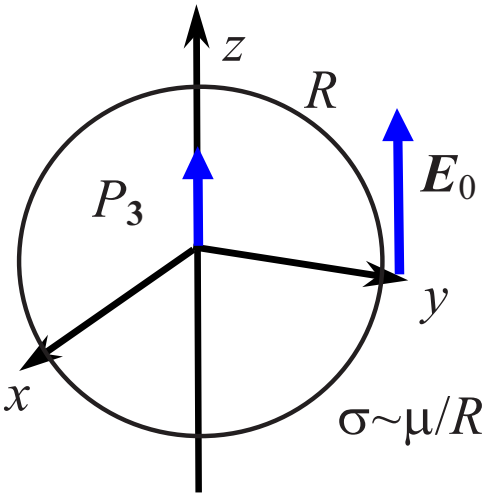

FIG. 7. (Color online) Geometry of a spherical particle.

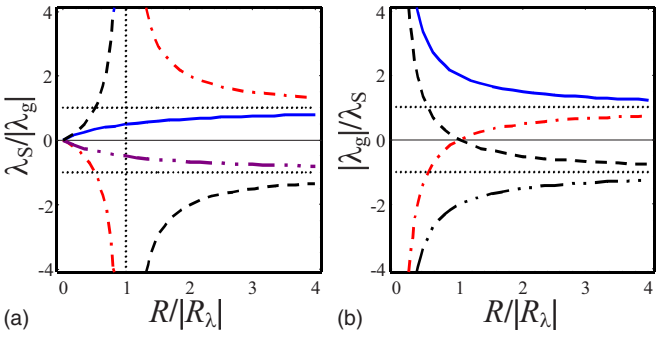

FIG. 8. (Color online) Characteristic length (a) $\lambda_S/|\lambda_g|$ and (b) $|\lambda_g|/\lambda_S$ vs sphere radius $R/|R_\lambda|$ for $\lambda_g>0$ and $R_\lambda<0$ (solid curves), $\lambda_g<0$ and $R_\lambda>0$ (dashed curves), $\lambda_g>0$ and $R_\lambda>0$ (dash-dotted curves), and $\lambda_g<0$ and $R_\lambda<0$ (double-dash-dotted curves).

$$\lambda_S^{-1}(R)=\frac{a_1^S}{g}+\frac{(2q_{12}^S+q_{11}^S)}{g}\frac{4\mu}{R}, \quad (22a)$$
$$P_d(R)=-(2d_{31}^S+d_{33}^S)\frac{2\mu}{R}\frac{\lambda_S}{g}. \quad (22b)$$

In the general case, length λ_S could be negative or positive because both signs of a_1^S could be encountered. Introducing the parameters $R_\lambda=-4(2q_{12}^S+q_{11}^S)\mu/a_1^S$ and $\lambda_g=g/a_1^S$, one obtains that $\lambda_S^{-1}(R)=\lambda_g^{-1}(1-R_\lambda/R)$. The normalized size dependence of characteristic length $\lambda_S/|\lambda_g|$ is shown in Fig. 8.

Application of the direct variational method for the Euler-Lagrange equation [Eq. (21)] solution leads to the conventional form of the free energy with renormalized coefficients:

$$G\approx\left\{\alpha_T[T-T_{sph}(R)]\frac{P_{3V}^2}{2}+a_{11}\frac{P_{3V}^4}{4}+a_{111}\frac{P_{3V}^6}{6}\right.$$
$$\left.-P_{3V}[E_0+E_{sph}(R)]\right\}. \quad (23)$$

Here, the surface polarization P_d in the boundary conditions leads to the appearance of the built-in electric field E_{sph} that induces an electretlike polar state at $R<R_{cr}$ and smears the phase transition point:

$$E_{sph}(R)\approx-\frac{6\mu}{R^2}(2d_{31}^S+d_{33}^S). \quad (24)$$

One can see from Eq. (24) that the built-in field is proportional to the surface stress tensor μ and piezoelectric coefficients d_{3j}^S. Internal electric field $E_{sph}(R)\sim1/R^2$ increases with decrease of particle radius and can lead to the particle self-polarization when it reaches the thermodynamics coercive field, like it was predicted for the thin films due to the misfit strain.[35] Thus, the assumption about the particle single-domain state used in our consideration looks self-consistent for sizes below 100 nm, in full agreement with experimental results.[10,11]

The transcendental equation for the Curie temperature $T_{sph}(R)$ at a given radius R, as well as for the critical radius $R_{sph}(T)$ at a given temperature T, which corresponds to the second order phase transition from ferroelectric to paraelectric phase (at $E_{sph}=0$) or electretlike state (at $E_{sph}\neq0$) acquires the form

$$a_R + \frac{\frac{3gn_d}{R^2(n_d+a_R)}\left[R\sqrt{\frac{n_d+a_R}{g}}\cosh\left(R\sqrt{\frac{n_d+a_R}{g}}\right)-\sinh\left(R\sqrt{\frac{n_d+a_R}{g}}\right)\right]}{\lambda_S\sqrt{\frac{n_d+a_R}{g}}\cosh\left(R\sqrt{\frac{n_d+a_R}{g}}\right)+\left(1-\frac{\lambda_S}{R}\right)\sinh\left(R\sqrt{\frac{n_d+a_R}{g}}\right)}=0, \tag{25}$$

where $a_R(T,R)=a_1(T)+(Q_{11}+2Q_{12})(4\mu/R)$. Note that the inequality $(Q_{11}+2Q_{12})>0$ holds for perovskites.

A. Phase transition in conventional ferroelectric nanospheres

Under the typical conditions $\varepsilon_e<10$ and $a_1(T)=\alpha_T(T-T_C)$, the transition temperature of a conventional ferroelectric has the form

$$T_{sph}(R)=T_C-(Q_{11}+2Q_{12})\frac{4\mu}{\alpha_T R}-\frac{3g}{R^2\alpha_T}\theta(\lambda_S,R), \tag{26a}$$

$$\theta(\lambda_S,R)=\frac{R\sqrt{n_d/g}\cosh(R\sqrt{n_d/g})-\sinh(R\sqrt{n_d/g})}{\lambda_S\sqrt{n_d/g}\cosh(R\sqrt{n_d/g})+(1-\lambda_S/R)\sinh(R\sqrt{n_d/g})}. \tag{26b}$$

At a given temperature T, the sphere critical radius $R_{cr}(T)$ should be found from the condition $T_{sph}(R_{cr})=T$.

For more detailed analyses of Eqs. (26), one should take into account that the length $\lambda_S^{-1}(R)=\lambda_g^{-1}(1-R_\lambda/R)$ depends on sphere radius R and parameters $R_\lambda=-(8q_{12}^S+4q_{11}^S)\mu/a_1^S$ and $\lambda_g=g/a_1^S$. Let us introduce the radius $R_\mu=(4Q_{11}+8Q_{12})\mu/\alpha_T T_C$, related to intrinsic surface stress, characteristic radius $R_d=\sqrt{g/n_d}$, and correlation radius $R_S=\sqrt{g/\alpha_T T_C}$ that coincides with order parameter correlation radius at zero temperature.[20]

Ferroelectric phase transition temperature T_{sph}/T_C vs radius R/R_S calculated from Eqs. (26) for different R_μ/R_S ratios and parameters R_λ/R_S and λ_g/R_S determining $\lambda_S^{-1}(R)=\lambda_g^{-1}(1-R_\lambda/R)$ radius dependence is depicted in Fig. 9.

At positive R_μ [that corresponds to the positive surface stress coefficient $\mu>0$, since $(Q_{11}+2Q_{12})>0$] the transition temperature increase $T_{sph}>T_C$ is possible at some region of negative lengths λ_g $(a_1^S<0)$ and/or positive R_λ (compare with enhancement for a cylinder). The situation $\mu<0$ might be possible at some special ambient conditions.

It is clear from Fig. 9 that the critical radius $R_{cr}(0)$ belongs to the region $3R_S<R_{cr}(0)<30R_S$ at positive λ_g/R_S, whereas for nanowires, the critical radius is much smaller at the same material parameters: $0.3R_S<R_{cr}(0)<3R_S$ (if any) [compare Figs. 3(a) and 9(a)]. The difference is related to the absence of depolarization field in nanowires and its presence in nanospheres.

Using the values $\mu=0.5-50$ N/m,[29,31] $g=10^{-11}-10^{-10}$ V m^3/C,[46,47] $2Q_{12}+Q_{11}=0.03$ m^4/C^2, $\alpha_T T_C\sim 4\times10^7-2\times10^8$ in SI units, $T_C\sim400-700$ K, and $n_d\sim4-0.04$, one can obtain for the perovskites such as $BaTiO_3$ and $PbTiO_3$ that $R_\mu\approx1.5-150$ nm for $BaTiO_3$ and $R_\mu\approx0.3-30$ nm for $PbTiO_3$, $R_S\approx0.4-1.6$ nm, and $R_d\sim0.1-1$ nm. Similarly to the case of nanowires, no restrictions are known for phenomenological parameters R_λ and λ_g, since the quantity a_1^S can take arbitrary values. Since typically $\exp(-R/R_d)\ll1$ for nanospheres of radius $R>0.5-5$ nm, we derived from Eqs. (26) that

$$T_{sph}(R)\approx T_C\left(1-\frac{R_Q}{R}-\frac{R_q^2}{R^2}\right), \tag{27a}$$

$$R_{cr}(T)\approx\frac{R_Q\pm\sqrt{R_Q^2+4(1-T/T_C)R_q^2}}{2(1-T/T_C)}, \tag{27b}$$

where $R_Q=(R_\mu+3R_S^2/\lambda_g)$ is determined by the intrinsic surface stress and bulk electrostriction and $R_q^2=-3R_S^2R_\lambda/\lambda_g$ is determined by the intrinsic surface stress, surface electrostriction, and correlation radius R_S (see Appendix A of Ref. 36).

Comparison of typical experimental data for the dependence of the Curie temperature $T_{sph}(d)$ on the size d of $BaTiO_3$ and $PbTiO_3$ nanoparticles with theoretical calculations on the basis of expression (26a), as well as a fit with the empirical Ishikava formula $T_{cr}(R)\approx T_C[1-R_0/(R-R_1)]$[48] is shown in Fig. 10.

It is seen from Fig. 10, that derived expression (27a) for $T_{sph}(R)$ fits the experimental points, as well as purely empirical Ishikava formulas at the same amount of fitting parameters.

It is worth to note that the critical sizes in ceramics and powder samples can vary significantly. It can be related to the ceramic preparation features, as well as with different mechanical and electrical boundary conditions for the grains of ceramics and particles of powder. In the framework of the proposed phenomenological theory, the values of surface intrinsic stress μ, surface energy expansion coefficient a_1^S, surface electrostriction q_{ij}^S, and depolarization factor $n_d\sim(1+2\varepsilon_e)^{-1}$ should differ for the ceramics and powder samples, prepared by different methods. Also, in order to consider the dielectric properties of the nanoparticle assembly, one has to take a concrete expression for their size distribution function.[45]

B. Size-induced ferroelectricity in incipient ferroelectric nanospheres

Using the Barrett formula for $a_1(T)$, the transition temperature induced by surface and size effects is given by

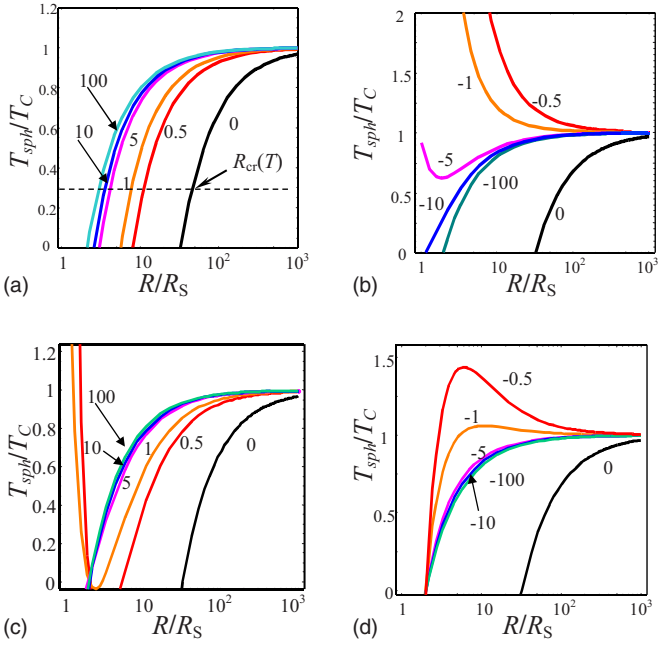

FIG. 9. (Color online) Transition temperature T_{sph}/T_C vs R/R_S calculated from Eqs. (26) for conventional ferroelectric at $R_d/R_S=0.1$, $R_\mu/R_S=2$, and [(a) and (b)] $R_\lambda/R_S=-2$ [(c) and (d)] and $R_\lambda/R_S=+2$ [(a) and (c)] for positive $\lambda_g/R_S=0,0.5,1,10,100$ and [(b) and (d)] negative $\lambda_g/R_S=0,-0.5,-1,-5,-10,-100$ (figures near the curves).

$$T_{sph}(R)=\frac{T_q}{2}\text{arccoth}^{-1}\left\{\frac{2}{T_q}\left[T_0-(Q_{11}+2Q_{12})\frac{4\mu}{\alpha_T R}-\frac{3g}{R^2\alpha_T}\theta(\lambda_S,R)\right]\right\}. \quad (28)$$

Here, $\theta(\lambda_S,R)$ is given by Eq. (26b). Using the asymptotic relation $[\text{arccoth}(x)]^{-1}\to x$ for $x\gg 1$, one can obtain that at temperatures $T\gg T_q/2$, Eq. (28) tends to Eqs. (26) after the substitution $T_C\to T_0$.

Below, we consider the size-induced ferroelectric phase in $KTaO_3$ nanospheres. We used Eq. (28) for the transition temperature; the electrostriction constant $(Q_{11}+2Q_{12})$ as taken from Ref. 44. Ferroelectric phase transition temperature T_{sph} vs sphere radius R for $KTaO_3$ is shown in Fig. 11. Part (a) corresponds to the case when characteristic length $|\lambda_S|\to+\infty$ ($\lambda_g\to+\infty$ and $q_{11}^S+2q_{12}^S=0$), so the polarization gradient can be neglected and the radius dependence of T_{sph} is caused by the surface stress via the bulk electrostriction effect. Parts (b) and (c) correspond to the case when both bulk electrostriction and polarization gradient contribute into the transition temperature, but surface electrostriction is absent, i.e., $q_{ij}^S=0$ and so $\lambda_S=\lambda_g=$const. It is clear that negative λ_g increases the transition temperature in comparison with the positive ones [compare (b) and (c)]. Part (d) shows the influence of surface electrostriction ($q_{ij}^S\neq 0$) on transition temperature T_{sph}. The cross point of the curves in plot (d) corresponds to the point $R=-R_\lambda$, where all characteristic length diverges in accordance with the equation $\lambda_S^{-1}(R)=\lambda_g^{-1}(1-R_\lambda/R)$.

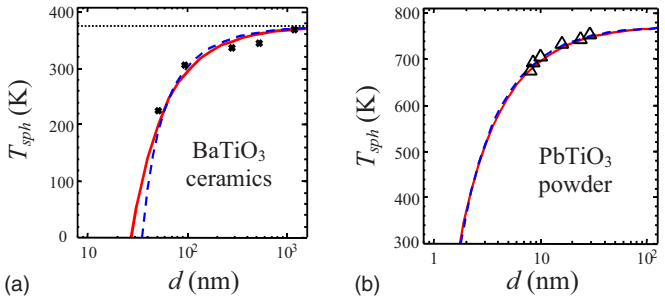

FIG. 10. (Color online) The dependence of the Curie temperature on the mean size d of the particles for (a) dense fine grained ceramics of $BaTiO_3$ (Ref. 10) and (b) nanopowder of $PbTiO_3$ obtained by electron paramagnetic resonance measurements (Ref. 11). Symbols are experimental data (Refs. 10 and 11) and the solid and dashed curves represent the fitting with Eq. (27a) and the Ishikawa formula, respectively. (a) $T_C=375$ K, $R_Q=19.6$ nm, and $R_q=15.5$ nm for Eq. (27a); $R_0=19$ nm and $R_1=16$ nm for the Ishikawa fit. (b) $T_C=773$ K, $R_Q=1$ nm, and $R_q=0.4$ nm for Eq. (27a); $R_0=0.9$ nm and $R_1=0.3$ nm for the Ishikawa fit.

It is clear from Fig. 11 that the effect of the appearance of ferroelectricity in spherical nanoparticles of incipient ferroelectrics is possible for negative intrinsic surface stress coefficient μ that stretches the particle, since $(Q_{11}+2Q_{12})>0$ [see plots (a), (c), and (d)]. At positive μ, the ferroelectric phase appears at negative length $\lambda_S(R)$ [see plot (b)], the latter being possible for the cases depicted in Fig. 8. Note that $\lambda_S(R)<0$ for arbitrary radii at negative length λ_g and radius R_λ, which is achieved under the conditions $a_1^S<0$ and $\mu(2q_{12}^S+q_{11}^S)<0$.

The prediction of size-induced ferroelectricity in $KTaO_3$ nanospheres of radius less than 1–5 nm (see vertical lines in Fig. 11) at room temperatures (see horizontal lines in Fig. 11) and aforementioned special conditions could be interesting. However, it is difficult to observe in comparison with nanowires, where analogous effect is expected at room temperatures and radius of 5–20 nm. The difference is related to the absence of depolarization field in nanowires in contrast to nanospheres with depolarization factor n_d chosen equal to $4\pi/3$.

Note that Abel has found that the hydrostatic pressure p higher than 2×10^9 Pa does not induce any ferroelectric phase in bulk $KTaO_3$. Moreover, reciprocal susceptibility increases, proving paraelectric phase stability.[49] This result is clear, since the electrostriction coefficient combination $(Q_{11}+2Q_{12})$ is positive and polarization gradient influence can be neglected in the bulk sample, so the positive value $(Q_{11}+2Q_{12})p$ only suppresses the appearance of the ordered state. This experimental fact confirms our conclusion about the absence of ferroelectricity at compressive surface stress, when $(Q_{11}+2Q_{12})\mu/R>0$.

Allowing for the facts that proposed the theoretical approach describing available experimental data[6,10,11] rather well (see Figs. 4 and 10), we would like to underline that simultaneous consideration of intrinsic surface stress, depolarization effects, and polarization gradient is the key for the adequate description of size-induced phase transitions in ferroelectric nanoparticles.

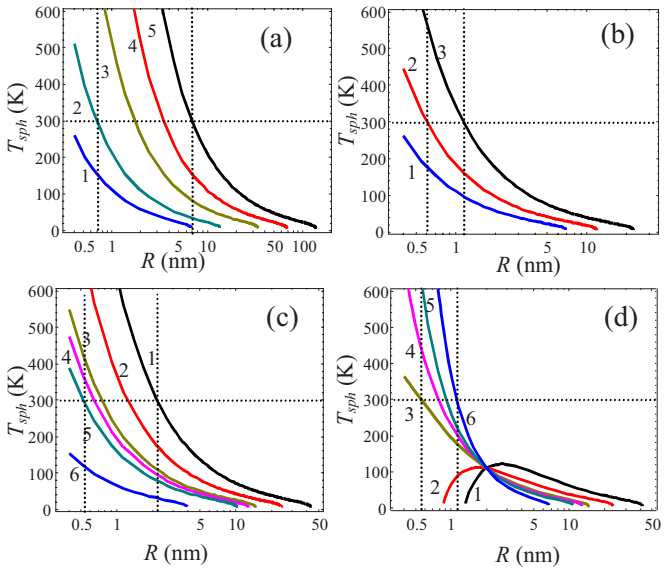

FIG. 11. (Color online) Ferroelectric phase transition temperature T_{sph} vs sphere radius R for $KTaO_3$ material parameters T_q =55 K, T_0=13 K, Curie-Weiss constant $C_{CW}=5.6\times10^4$ K, and $Q_{11}+2Q_{12}=0.041$ m^4/C^2; gradient coefficient $g=10^{-10}$ V m^3/C in SI units and $n_d=4\pi/3$. (a) $|\lambda_g|\to+\infty$, $R_\lambda=0$, and negative surface stress values μ: −1, −2, −5, −10, −20 N/m (curves 1, 2, 3, 4, 5); (b) $\mu=1$ N/m, $R_\lambda=0$, and negative lengths $\lambda_g=-0.8,-0.6,-0.4$ nm (curves 1, 2, 3); (c) $\mu=-2$ N/m, $R_\lambda=0$, and lengths $\lambda_g=-0.4,-1,-10,10,3,1$ nm (curves 1, 2, 3, 4, 5, 6); (d) $\mu=-2$ N/m, $R_\lambda=+2$ nm, and $\lambda_g=-0.4,-1,-10,10,3,1$ nm (curves 1, 2, 3, 4, 5, 6).

The polarization gradient influence manifests itself via the transition temperature dependence on R_S, where R_S is the bulk material correlation radius at zero temperature. It is worth to note that in the majority of the figures (see Figs. 3, 5, and 9), we represented the transition temperature via the ratio R/R_S. For most of the cases, essential increase of transition temperature corresponds to the radii less than several R_S even at large R_μ value, related to intrinsic surface stress.

VI. DISCUSSION

The properties of magnetic and elastic nanoparticles could be considered in the same way as it has been shown in detail for ferroelectric nanoparticles. Under the favorable conditions, the approximate formulas [Eq. (4)] can be applied for the calculation of the transition temperature and phase diagrams of all primary ferroics, as it was declared in Sec. II.

Really, in the case of infinite cylindrical magnetic nanoparticle with order parameter aligned along its axis, the depolarization factor is zero and thus inner field E_3^d is absent. The gradient contribution into the renormalization of $a_{ij}(T)$ can be estimated as $g/(\lambda_S R)\cong10-0.1$ cgsm units for monodomain ferromagnetic nanoparticles with radius of curvature $R=5-50$ nm and gradient coefficient square root $\sqrt{g}\sim50$ nm and characteristic length $\lambda_S=50-500$ nm.[22,39] The estimation of the surface stress contribution to the renormalization of $a_{ij}(T)$ gives $2Q_{lkij}L_{lk}(\mu/R)\cong10^2-10$ cgsm units at $R=5-50$ nm, $L_{lk}\sim1$, and $\mu\cong5\times10^4$ dyn/cm for bulk magnetostriction coefficients $Q_{lkij}\sim10^{-9}$ cm^3/erg typical for rare-earth alloys.[50] Thus, the striction renormalization may be comparable to or essentially larger than the aforementioned gradient contribution for radii 5 nm$<R<$50 nm, making Eqs. (3) and (4) valid for magnetic nanorods. The estimations had shown that in small nanoparticles, magnetization could appear when it is absent in the bulk, explaining qualitatively experimental results.[5]

The estimations made in the end of Sec. II have shown the possibility of appearance of ferroelectricity in the incipient ferroelectric nanoparticles that has been confirmed by rigorous calculations in Secs. IV and V. The preferable conditions for the observation of this phenomenon could be as follows:

(i) The best nanoparticle shape is a long nanorod with radius less than several tens of nanometers that provides vanishing depolarization field and strong surface stress effect. For incipient ferroelectric nanorods of perovskite symmetry ($KTaO_3$ or $SrTiO_3$), effect is possible even at room temperature if $\mu Q_{12}<0$, i.e., when $\mu>0$ since $Q_{12}<0$. An additional desirable condition is the negative length λ_S, appearing even at positive extrapolation length $\lambda_g>0$ when nanoparticle radius $R<R_\lambda$, the latter being possible if $\mu q_{12}^S<0$.

(ii) For spherical nanoparticles, the effect of the appearance of ferroelectricity is possible at radii less than several nanometers and it is difficult to observe at room temperatures in contrast to nanorods. The difference is related to the absence of depolarization field in nanowires in contrast to nanospheres. Hypothetically, size-driven ferroelectric phase transition in nanospheres is possible if $\mu(Q_{11}+2Q_{12})<0$, i.e., when $\mu<0$, since $(Q_{11}+2Q_{12})>0$ for perovskites. Another possibility is the change of the length λ_S sign at some value of the nanoparticle radius that is achieved when $\mu(2q_{12}^S+q_{11}^S)<0$.

The experimental justification of the theoretical forecast is extremely desirable.

ACKNOWLEDGMENT

Research was partially supported (MDG and EAE) by the Science & Technology Center in Ukraine, Project No. 3898.

*Corresponding authors.
†morozo@i.com.ua. Permanent address: V. Lashkarev Institute of Semiconductor Physics, NAS of Ukraine, 41, pr. Nauki, 03028 Kiev, Ukraine.
‡glin@materials.kiev.ua
§eliseev@i.com.ua

[1] V. K. Wadhawan, *Introduction to Ferroic Materials* (Gordon and Breach, New York, 2000).
[2] E. Roduner, *Nanoscopic Materials: Size-dependent Phenomena* (RSC Publishing, Cambridge, 2006).

[3] Michael G. Cottan, *Linear and Nonlinear Spin Waves in Magnetic Films and Super-Lattices* (World Scientific, Singapore, 1994).
[4] D. R. Tilley, in *Ferroelectric Thin Films*, edited by C. Paz de Araujo, J. F. Scott, and G. W. Teylor (Gordon and Breach, Amsterdam, 1996), p. 11.
[5] Y. Nakal, Y. Seino, T. Teranishi, M. Miyake, S. Yamada, and H. Hori, Physica B **284**, 1758 (2000).
[6] D. Yadlovker and S. Berger, Phys. Rev. B **71**, 184112 (2005).
[7] A. N. Morozovska, E. A. Eliseev, and M. D. Glinchuk, Phys. Rev. B **73**, 214106 (2006).
[8] A. N. Morozovska, E. A. Eliseev, and M. D. Glinchuk, Physica B **387**, 358 (2007).
[9] M. H. Frey and D. A. Payne, Phys. Rev. B **54**, 3158 (1996).
[10] Z. Zhao, V. Buscaglia, M. Viviani, M. T. Buscaglia, L. Mitoseriu, A. Testino, M. Nygren, M. Johnsson, and P. Nanni, Phys. Rev. B **70**, 024107 (2004).
[11] E. Erdem, H.-Ch. Semmelhack, R. Bottcher, H. Rumpf, J. Banys, A. Matthes, H.-J. Glasel, D. Hirsch, and E. Hartmann, J. Phys.: Condens. Matter **18**, 3861 (2006).
[12] F. Wiekhorst, E. Shevchenko, H. Weller, and J. Kotzler, Phys. Rev. B **67**, 224416 (2003).
[13] M. Respaud, J. M. Broto, H. Rakoto, and A. R. Fert, Phys. Rev. B **57**, 2925 (1998).
[14] N. A. Pertsev, A. K. Tagantsev, and N. Setter, Phys. Rev. B **61**, R825 (2000).
[15] W. L. Zhong, Y. G. Wang, P. L. Zhang, and D. B. Qu, Phys. Rev. B **50**, 698 (1994).
[16] C. L. Wang and S. R. P. Smith, J. Phys.: Condens. Matter **7**, 7163 (1995).
[17] I. Rychetsky and O. Hudak, J. Phys.: Condens. Matter **9**, 4955 (1997).
[18] J. Zhang, Zh. Yin, M.-Sh. Zhang, and J. F. Scott, Solid State Commun. **118**, 241 (2001).
[19] L. D. Landau and E. M. Lifshits, *Electrodynamics of Continuous Media* (Butterworth-Heinemann, Oxford, 1980).
[20] M. E. Lines and A. M. Glass, *Principles and Applications of Ferroelectrics and Related Phenomena* (Clarendon, Oxford, 1977).
[21] Ch. Kittel, *Introduction to Solid State Physics* (Chapman and Hall, London, 1956).
[22] M. I. Kaganov and A. N. Omelyanchouk, Zh. Eksp. Teor. Fiz. **61**, 1679 (1971) [Sov. Phys. JETP **34**, 895 (1972)].
[23] R. Kretschmer and K. Binder, Phys. Rev. B **20**, 1065 (1979).
[24] L. D. Landau and E. M. Lifshitz, *Theoretical Physics* (Butterworth-Heinemann, Oxford, UK, 1998), Vol. 7.
[25] O. Song, C. A. Ballentine, and R. C. O'Handley, Appl. Phys. Lett. **64**, 2593 (1994).
[26] M. D. Glinchuk and A. N. Morozovska, J. Phys.: Condens. Matter **16**, 3517 (2004).
[27] A. M. Bratkovsky and A. P. Levanyuk, Phys. Rev. Lett. **94**, 107601 (2005).
[28] V. I. Marchenko and A. Ya. Parshin, Zh. Eksp. Teor. Fiz. **79**, 257 (1980) [Sov. Phys. JETP **52**, 129 (1980)].
[29] V. A. Shchukin and D. Bimberg, Rev. Mod. Phys. **71**, 1125 (1999).
[30] K. Uchino, E. Sadanaga, and T. Hirose, J. Am. Ceram. Soc. **72**, 1555 (1989).
[31] W. Ma, M. Zhang, and Z. Lu, Phys. Status Solidi A **166**, 811 (1998).
[32] Z. H. Zhou, X. S. Gao, John Wang, K. Fujihara, S. Ramakrishna, and V. Nagarajan, Appl. Phys. Lett. **90**, 052902 (2007).
[33] N. A. Pertsev, A. G. Zembilgotov, and A. K. Tagantsev, Phys. Rev. Lett. **80**, 1988 (1998).
[34] M. D. Glinchuk, E. A. Eliseev, and V. A. Stephanovich, Physica B **332**, 356 (2002).
[35] M. D. Glinchuk, A. N. Morozovska, and E. A. Eliseev, J. Appl. Phys. **99**, 114102 (2006).
[36] A. N. Morozovska, M. D. Glinchuk, and E. A. Eliseev, arXiv:cond-mat/0703652.
[37] A. N. Morozovska, S. V. Kalinin, and E. A. Eliseev, Appl. Phys. Lett. **89**, 192901 (2006).
[38] P. Paruch, T. Giamarchi, T. Tybell, and J.-M. Triscone, J. Appl. Phys. **100**, 051608 (2006).
[39] G. Catalan, J. F. Scott, A. Schilling, and J. M. Gregg, J. Phys.: Condens. Matter **19**, 022201 (2007).
[40] R. Landauer, J. Appl. Phys. **28**, 227 (1957).
[41] E. D. Mishina, N. E. Sherstyuk, V. O. Valdner, A. V. Mishina, K. A. Vorotilov, V. A. Vasiliev, A. S. Sigov, M. P. De Santo, E. Cazzanelli, R. Barberi, and Th. Rasing, Solid State Phys. **48**, 1133 (2006).
[42] F. D. Morrison, Y. Luo, I. Szafraniak, V. Nagarajan, R. B. Wehrspohn, M. Steinhart, J. H. Wendroff, N. D. Zakharov, E. D. Mishina, K. A. Vorotilov, A. S. Sigov, S. Nakabayashi, M. Alexe, R. Ramesh, and J. F. Scott, Rev. Adv. Mater. Sci. **4**, 114 (2003).
[43] J. H. Barrett, Phys. Rev. **86**, 118 (1952).
[44] H. Uwe and T. Sakudo, Phys. Rev. B **15**, 337 (1977).
[45] M. D. Glinchuk and A. N. Morozovska, Phys. Status Solidi B **238**, 81 (2003).
[46] D. A. Scrymgeour, V. Gopalan, A. Itagi, A. Saxena, and P. J. Swart, Phys. Rev. B **71**, 184110 (2005).
[47] G. B. Stephenson and K. R. Elder, J. Appl. Phys. **100**, 051601 (2006).
[48] K. Ishikava, K. Yoshikava, and N. Okada, Phys. Rev. B **37**, 5852 (1988).
[49] W. R. Abel, Phys. Rev. B **4**, 2696 (1971).
[50] Ce Wen and Ming Li, Phys. Rev. B **63**, 144415 (2001).